Energy Level Gradients from Surface to Bulk in Hybrid Metal-Halide Perovskite Thin Films

Sean A. Bourelle,[1] Xie Zhang,[2,3] Sascha Feldmann,[1] Baiyu Zhang,[2] Angus Mathieson,[1] Lissa Eyre,[1] Haralds Abolins,[1] Thomas Winkler,[1,4] Chris G. Van de Walle,[2,*] and Felix Deschler[5,†]

[1] *Cavendish Laboratory, University of Cambridge, Cambridge, CB3 0HE, United Kingdom*
[2] *Materials Department, University of California, Santa Barbara, California 93106-5050, USA*
[3] *School of Materials Science and Engineering, Northwestern Polytechnical University, Xi'an 710072, China*
[4] *Department of Physics and Astronomy, Aarhus University, Aarhus C, 8000, Denmark*
[5] *Institute for Physical Chemistry, University of Heidelberg, 69120 Heidelberg, Germany*

(Received 14 December 2023; revised 14 May 2024; accepted 2 July 2024; published 26 July 2024)

Variations in local strain, defect densities, and composition of hybrid metal-halide perovskites have been reported to create heterogeneous energy landscapes in thin films, which impact charge-carrier diffusion and recombination dynamics. Here, we employ one- and two-photon transient absorption spectroscopy to selectively probe the dynamics of charge carriers from surface and bulk regions of methylammonium lead bromide thin films. Differences in the transient absorption spectra indicate that an energy gradient of approximately 100 meV is formed between the higher band-gap surface and lower band-gap bulk regions. Thus, during their lifetime, photoexcited carriers move away from the surface to recombine in the bulk, where our experiments detect long-lived charge populations despite the significant band splitting that has conventionally been assumed to inhibit efficient radiative recombination. Supported by first-principles calculations, we demonstrate that bright emission can still arise from the bulk with states that occupy a wide range of momenta in the vicinity of the band extrema, which show strong dipole transitions. Our results report that photoexcitations in the hybrid perovskites avoid defect-rich surface regions, and that particularly strong emission is generated from accumulated excitation populations in the bulk.

DOI: 10.1103/PRXEnergy.3.033001

I. INTRODUCTION

Insights on the local distribution of energy levels, symmetry, and nature of photoexcited states in hybrid metal-halide perovskite semiconductors are required for the efficient operation of hybrid perovskite optoelectronic devices [1]. Further, charge extraction efficiencies require detailed knowledge of the band alignment between the hybrid perovskite surface and connected extraction layers [2,3]. Efficiencies of high-performance devices can be enhanced even further by optimizing photoexcitation dynamics, e.g., by improved open-circuit voltages from reduced recombination [4,5], and avoidance of interfacial charge-carrier buildup [6]. Metal-halide hybrid perovskites are direct-band-gap semiconductors with tunable band gaps depending on the chemical composition. For instance, cubic methylammonium lead bromide ($MAPbBr_3$) has a band gap of approximately 2.34 eV located at the high-symmetry **k**-point *R*. However, the presence of the dipolar MA molecule in the material breaks the exact inversion symmetry. Combining the lack of inversion symmetry and strong spin-orbit coupling of the heavy Pb and Br ions that constitute the band edges, the so-called Rashba effect arises, leading to momentum splitting at the band edges [7]. As a result, the band gap becomes slightly indirect. Long carrier lifetimes in the metal-halide perovskites, which support efficient charge extraction, have been claimed to originate from the Rashba splitting effects in the electronic band structure. Long lifetimes often correspond to low emission efficiency if competing nonradiative losses occur. However, reports of high luminescence yields [8,9] and detailed analysis of rate equations [10] suggest efficient radiative recombination [11], which indicates that defects have surprisingly little impact on photoexcitation.

Insights on photoexcitation dynamics have been gained with transient photoluminescence and transient absorption techniques. The underlying optical transitions in

*Contact author: vandewalle@mrl.ucsb.edu
†Contact author: deschler@uni-heidelberg.de

halide perovskites have commonly been analyzed based on optical selection rules that assume the Rashba-split bands are labeled by well-defined values of the total angular momentum projection m_j. However, first-principles calculations have shown that the combination of strong spin-orbit coupling and structural distortions of the inorganic lattice—likely induced by the dipolar methylammonium molecule—leads to a complex spin texture [12,13]. Previous reports utilizing photoluminescence measurements [14] have employed one-photon and two-photon photoexcitation to populate states near the surface or within the bulk [Fig. 1(a)] and have gained insights on how luminescence is generated under these conditions. However, insights into the surface and bulk optical band gap and the photoexcitation populations are challenging [15,16]. We now combine the concept of selective surface excitation and bulk excitation with one- and two-photon transient absorption spectroscopy [Figs. 1(a) and 1(b)], which can be employed as a sensitive probe for optical transitions and excitation dynamics at the surface and in the bulk of thin films [17,18]. We employ this method to gain detailed insights into the energy level structure and photoexcitation dynamics at the surface and in the bulk regions of $MAPbBr_3$ thin films, which was not possible with previous experiments.

With our approach, we report that heterogeneity exists in the electronic states throughout hybrid metal-halide perovskite thin films and demonstrate that the surface of hybrid perovskite films shows larger band gaps than the bulk, leading to carrier funneling into the bulk region of thin films [19]. There, radiative recombination occurs from Rashba-split bands, which we find to show larger splitting than at the surface of perovskite films. Our findings provide a rationale for the unusual surface defect tolerance of hybrid perovskites and suggest limitations on charge extraction from the bulk due to energy barriers. We employ first-principles calculations to identify the local orientation of MA molecules and local strain as a potential structural origin for the observed local energy level differences throughout the hybrid perovskite films, which provides guidelines for optimization of hybrid perovskite surfaces for optimal device performance.

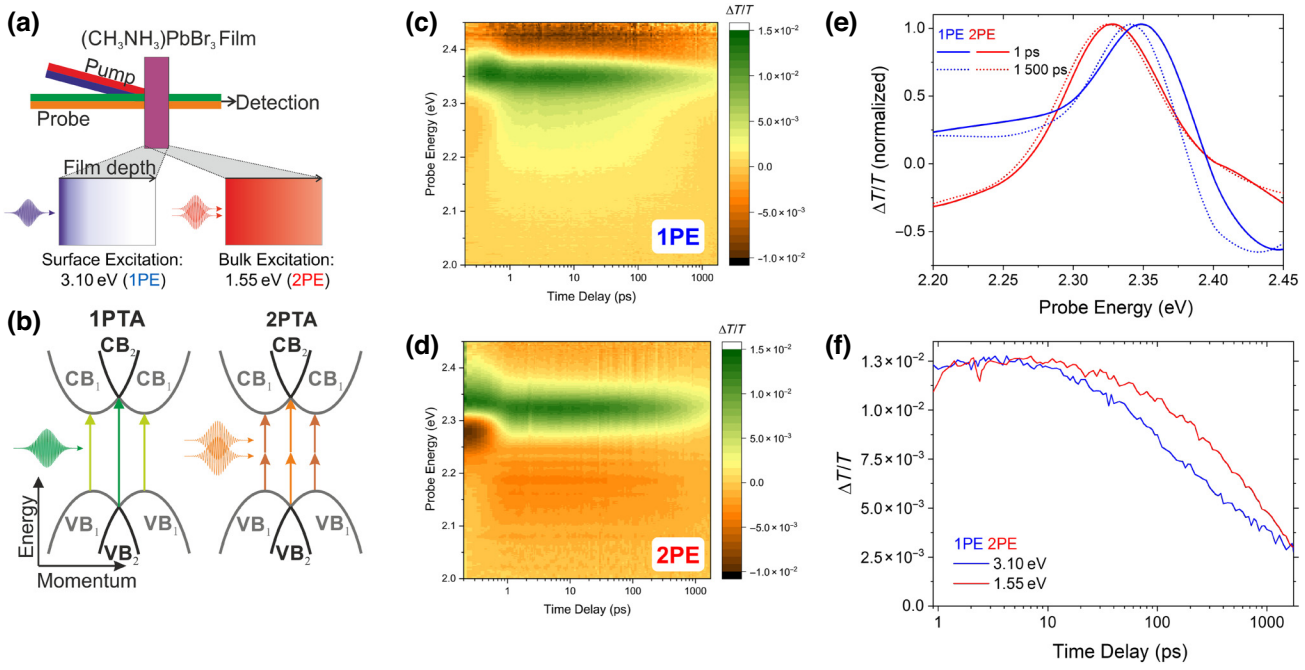

FIG. 1. (a) Experimental concept of one-photon and two-photon optical spectroscopy. Schematic of the pump-probe scheme with one-photon excitation (1PE) at 3.1 eV and two-photon excitation (2PE) at 1.55 eV. Probe photon energies are centered at 2.2 eV (visible range) for one-photon transient absorption (1PTA), and at 1.15 eV (near-infrared region) for two-photon transient absorption (2PTA) to study photoexcitation energies and dynamics in a thin film (∼500 nm) of $MAPbBr_3$. Below: sketch of initial photoexcited carrier density as a function of film depth for 1PE surface excitation (blue) and 2PE bulk excitation (red). (b) Sketch of the conduction bands (CBs) and valence bands (VBs) in hybrid perovskites near a symmetry point, and the transitions that are probed with 1TPA and 2PTA. The shaded arrows indicate the transitions between the outer branches (VB_1 to CB_1) while full colors indicate the higher energetic transition starting at the symmetry point (involving VB_2 or CB_2). (c),(d) Maps of the energy-resolved 1PTA response following 1PE surface excitation and 2PE bulk excitation at fluences of 6 and 45 μJ/cm^2, respectively. (e) 1PTA spectra at 1-ps time delay following 1PE surface excitation (blue) and 2PE bulk excitation (red). (f) Kinetics of the ground-state bleach signal at a probe energy of 2.34 eV following 1PE (blue) and 2PE (red).

II. RESULTS AND DISCUSSION

First, we study the recombination dynamics of photoexcited carriers with one-photon transient absorption (1PTA) on a thin film of $MAPbBr_3$, following one-photon surface excitation (1PE) at 3.10 eV and two-photon bulk excitation (2PE) at 1.55 eV with linearly polarized laser pulses [Fig. 1(a), see experimental details in the Supplemental Material [20]]. Using one-photon excitation, excitations are dominantly photogenerated near the surface of the film (∼50 nm), while using two-photon excitation, a more uniform excitation density throughout the film is created (see Fig. S1 in the Supplemental Material [20]).

We record maps of the energy-resolved transient absorption response for 1PE and 2PE [Figs. 1(c) and 1(d)]. Note that the comparable maximum value of the signal amplitude indicates that we have created comparable excitation densities, despite the typical difference in excitation fluence for 1PE and 2PE conditions. We find unexpected differences in the energy position of the main bleach feature, and the recombination dynamics of the excited states. To analyze this further, we compare spectral shapes and kinetics. The shapes of 1PTA spectra at a time delay of 1 ps following 1PE [Fig. 1(e), blue line] and 2PE [Fig. 1(e), red line] show distinct differences. The 1PE-1PTA signal, arising from photoexcitations formed closer to the surface of the film, is dominated by transient reflectivity changes [27], giving a more derivativelike shape, as we further confirm by transient reflectivity measurements (see Fig. S2 in the Supplemental Material [20]). In these reflection-dominated spectra, the energy of the optical absorption transition is located close to the zero-crossing of the 1PE-1PTA spectra, which we find at around 2.38 eV. On the other hand, the 2PE-1PTA signal, arising from photoexcitations that are more homogenously distributed throughout the bulk of the film, shows a less derivativelike shape, with a ground-state bleach (GSB) peak at 2.32 eV. Thus, we find different values for the main optical transition under 1PE and 2PE conditions. One possible mechanism is that the optical band-gap energy is lower in the bulk than at the surface of our hybrid perovskite thin films.

The strength of the GSB and reflectivity signal in our transient absorption measurements give a measure for the overall carrier density, and hence provide a method to track the carrier recombination within the film. Transient absorption is integrated here over the excitation density throughout the film. We have ensured comparable peak signal intensities for $\Delta T/T$ under 1PE and 2PE conditions, which translates to comparable photoexcited excitation populations immediately after excitation. However, we find that the recombination kinetics is different under 1PE (surface) and 2PE (bulk) conditions [Fig. 1(f)]. Initially after photoexcitation, up to 200 ps, carrier recombination following 1PE (blue) is faster than for 2PE (red). Then, carrier recombination following 1PE becomes slower than for 2PE, and both kinetics converge around 1 ns. We further confirm the impact of 1PE vs 2PE conditions on recombination dynamics with time-resolved photoluminescence measurements and simulate the spatial excitation profiles (see Figs. S3–S6 in the Supplemental Material [20]).

However, 1PTA and photoluminescence are not directly sensitive to differences in local carrier distribution between surface and bulk. Thus, we employ two-photon transient absorption (2PTA) spectroscopy to separately probe the optical transition energies and dynamics of surface and bulk excited states. In short, the 2PTA technique uses the same pump-probe principle as 1PTA. However, optical transitions are probed by the simultaneous absorption of two photons, thus probing transitions at the sum of the two probe photon energies. The linear absorption and 1PTA signals of our hybrid metal-halide perovskites are around 2.2 eV, in the visible range [Fig. 1(e)]. Accordingly, we detect 2PTA signals at probe photon energies around 1.1 eV [Figs. 2(a) and 2(b)]. There are small overlaid signals from 1PTA signals in this probe range, likely from defect or free-carrier intraband excitation. However, since 2PTA signals scale quadratically with probe fluence, while 1PTA signals scale linearly, we can use a probe fluence series for correction and obtain the pure 2PTA signals (see the experimental details in the Supplemental Material [20]).

The energy-resolved maps of the 2PTA response of the material show broad bleach signals [Figs. 2(a) and 2(b)], which we assign to the two-photon probed optical band-edge transition at twice the probe photon energy (i.e., in the energy range 2.1–2.6 eV). Here, a redshift of the optical transition for 2PE vs 1PE is clearly visible. To analyze this further, we compare in the following selected spectra and kinetics.

The 2PTA spectra following 1PE, forming photoexcitations near the surface of the film [Fig. 2(d), blue lines], shows a positive bleach signal at an energy of 1.2 eV, relating to a two-photon probed optical transition at 2.4 eV. Owing to the bulk-sensitive nature of our 2PTA measurement, the spectrum is not much affected by reflectivity changes that we have seen when probing after surface excitation with 1PTA. We note that the energy of this bleach peak agrees with the transition energy of around 2.38 eV that we had determined in the 1PE-1PTA spectra [Fig. 2(c), blue lines].

The 2PTA signal following 2PE, in which we excite a more uniform carrier distribution throughout the bulk of the film, shows a bleach signal with a peak centered around 2.28 eV [Fig. 2(d), red line]. This energy is about 40 meV further below the redshifted transition that we observed in 1PTA under 2PE (bulk) excitation [Fig. 2(c), red line], suggesting that our 2PTA gives a clearer signal on these low-energy transitions. We note that the respective optical transition is around 100 meV lower in energy than the transitions we found after 1PE (surface) excitation [Fig. 2(d),

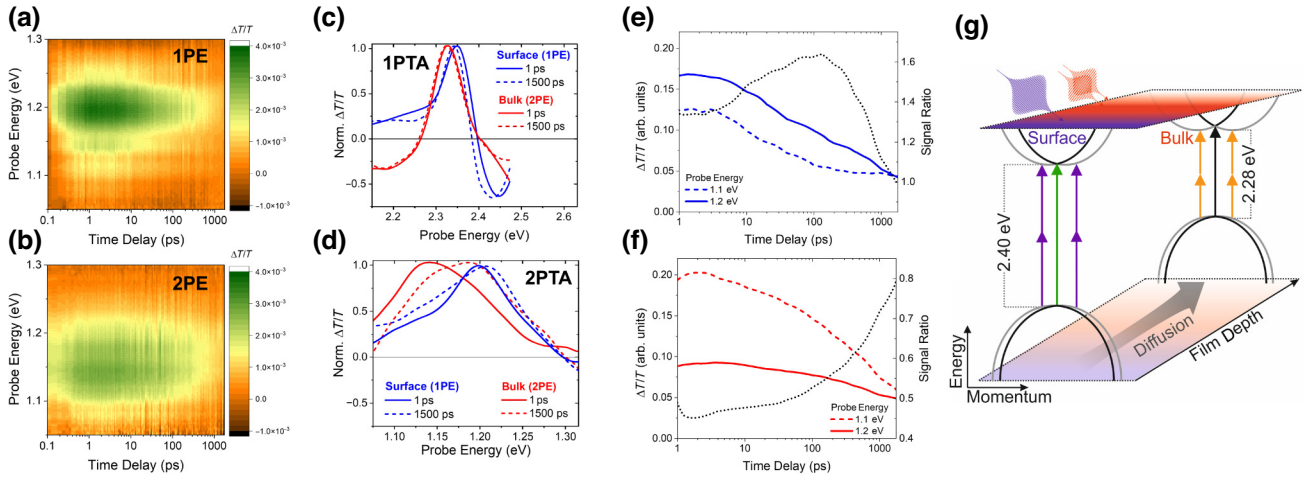

FIG. 2. (a),(b) Maps of the energy-resolved 2PTA response following 1PE surface excitation at 3.1 eV and 2PE bulk excitation at 1.55 eV. (c),(d) TA spectra for one-photon (1PTA) and two-photon (2PTA) probing following 1PE and 2PE, taken at time delays as indicated. (e),(f) Integrated 2PTA kinetics in the energy range around 1.1 eV (dotted line), which we attribute to signals from the bulk, and 1.2 eV (solid line), which we attribute to signals from the surface region, following 1PE and 2PE. (g) Sketch of the energy alignment of the observed optical transitions and carrier dynamics at surface and bulk regions of the studied hybrid perovskite films. The transition energies are extracted from our measured TA spectra shown in (c),(d) at a time delay of 1 ps.

blue line]. These results show that optical transitions in the surface and bulk regions occur at different energies, and that the lowest-energy optical transitions of the studied hybrid perovskite thin films are in the bulk region.

Using 2PTA spectra at different time delays, we resolve the impact of the energy gradients on the dynamics of photoexcited surface and bulk states. In the 1PE-2PTA spectra, at a time delay of 1500 ps, as carriers have moved away from the region of surface excitation and into the bulk [Fig. 2(d), blue line], we find a rise in the low-energy range around 1.15 eV, which we have identified previously to probe mostly bulk states. The small difference to the bulk vs surface peak separation determined with 1PTA is within the error of the experimental setup. We attribute this to a preferential diffusion of photoexcitations away from the surface and into the bulk region. We obtain the dynamics of these carrier dynamics by integrating the 2PTA spectrum in the spectral regions around 1.1 eV (bulk) and 1.2 eV (surface) [Fig. 2(e)]. The signal at 1.2 eV, which probes bulk excitations, initially shows a higher rate of carrier recombination [Fig. 2(e)], which levels out at later times as further photoexcitations diffuse from the surface into the bulk with time delays longer than around 100 ps.

Following 2PE (bulk), this leveling out of recombination kinetics is not observed and carrier recombination in the bulk remains faster than at the surface [Fig. 2(f)]. Accordingly, the 2PE-2PTA spectrum at a time delay of 1500 ps [Fig. 2(d), red line] contains increasing contributions of signals from the surface region, which is reflected by the rise in signal at 1.2 eV, despite the initially uniform excitation distribution (see Fig. S1 in the Supplemental Material [20]). We assign this to a slower decay of excitations that remain near the surface. In conclusion, we find two main observations from our 2PTA experiments: (i) energy gradients exist in the optical transitions between surface and bulk, with lower-energy transitions in the bulk region; (ii) photoexcitations diffuse into the bulk with increasing time delay, where they recombine with higher rates than at the surface.

To gain insights into the origin of the energy level variations at the surface and in the bulk, we compare our experimental observations with first-principles calculations. Owing to the combination of strong spin-orbit coupling and structural distortions induced by the dipolar methylammonium molecule, the picture in which the Rashba-split bands are characterized by sharp values of m_j is oversimplified, and therefore transitions between two bands cannot be described by simple optical selection rules that could potentially be addressed by single- or two-photon absorption [12,13].

To explore the material origin of our observations, we compute the electronic structure of $MAPbBr_3$ from first principles. The rotation barrier of MA in $MAPbBr_3$ is substantial (11 kJ mol^{-1}) [28,29], and diffraction experiments have shown that the MA molecules in bulk $MAPbBr_3$ are preferentially oriented along [110] at room temperature [30,31]. However, the picture may be different near the surface: studies of $MAPbI_3$ have suggested that there exists surface band bending [32]. Such surface band bending acts as an electric field that is significantly stronger than the coercive field (~0.6 kV cm^{-1}) [33] induced by the dipolar MA molecule. Thus, the MA molecule will reorient toward [001] at the surface to align with the electric field. We therefore perform first-principles

computations to determine the expected electronic structure using these organic cation orientations for the surface and the bulk (see the computational details in the Supplemental Material [20]).

From our calculations, we find two key differences in the optical transitions between surface and bulk regions. First, the MA reorientation gives rise to a difference in the transition energy between conduction and valence band extrema of the bulk and surface regions, as seen by the transition energy plotted for a slice ($k_z = 0.5$ in units of $2\pi/a$) of $\mathbf{k}$ points in the Brillouin zone with the respective ("bulk" and "surface") MA orientations [Figs. 3(a) and 3(c)]. Second, the Rashba splitting at the surface is significantly weaker than that in the bulk [Figs. 3(b) and 3(d) insets]; the corresponding Rashba coefficients for the lowest conduction band ($\alpha_R = 2\Delta E/\Delta k$, where ΔE and Δk are the energy and momentum splittings, respectively) are 2.34 eVÅ for bulk and 1.40 eVÅ for surface. Typically, one would expect surface effects to enhance the Rashba splitting due to a breaking of inversion symmetry. However, in the case of hybrid metal-halide perovskites, we have previously shown that the strength of the Rashba splitting directly correlates with the distortion of the $[PbBr_6]^{4-}$ octahedra [12,13], which can be characterized by the standard deviation of the Br–Pb–Br bond angles from 90°. When the molecule is oriented along [110], the distortion of

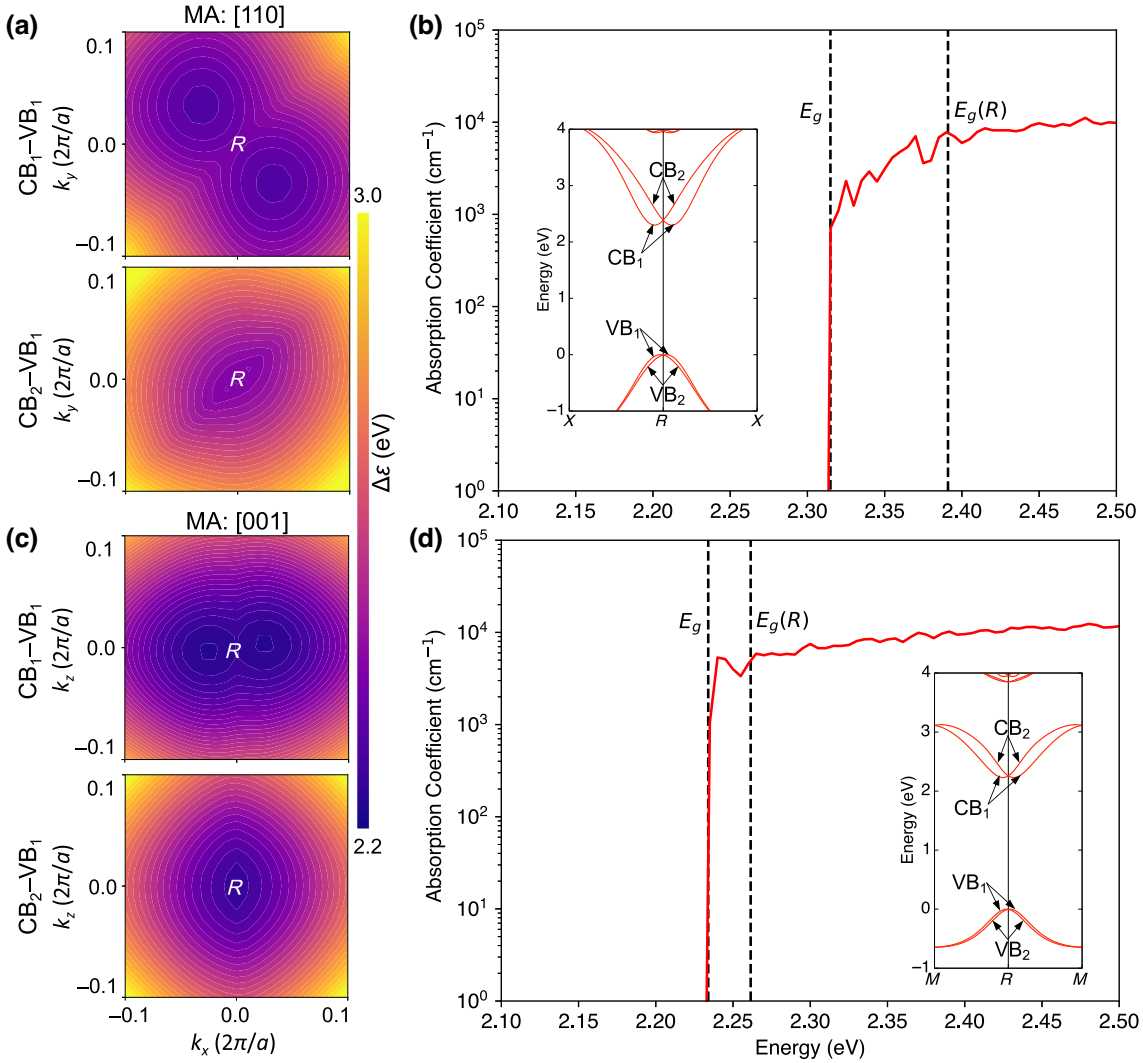

FIG. 3. Calculated band structure and one-photon absorption of $MAPbBr_3$. (a) Transition energy between the lowest two CBs and the highest VB [as defined in (b)] for a slice ($k_z = 0.5$ in units of $2\pi/a$) of $\mathbf{k}$ points in the Brillouin zone with MA oriented along [110]. The coordinates of the $\mathbf{k}$ points are defined relative to the R point (0.5, 0.5, 0.5). (b) Absorption coefficient of $MAPbBr_3$ with MA oriented along [110]. E_g refers to the lowest energy band gap and $E_g(R)$ denotes the band-gap energy at $\mathbf{k} = R$. (c) Transition energy between the lowest two CBs and the highest VB for a slice ($k_y = 0.5$ in units of $2\pi/a$) of $\mathbf{k}$ points in the Brillouin zone with MA oriented along [001]. (d) Absorption coefficient of $MAPbBr_3$ with MA oriented along [001]. The insets in (b) and (d) show the band structures of $MAPbBr_3$ along the $\mathbf{k}$-point path where the Rashba splitting is most pronounced.

the $[PbBr_6]^{4-}$ octahedra is much larger than that in the case with the MA oriented along [100] due to interactions between the dipolar MA cation and the inorganic lattice. Hence, the Rashba splitting is reduced when MA is reoriented along [001] [Fig. 3(d), inset].

To rationalize why radiative recombination still efficiently occurs within the bulk, despite the larger Rashba splittings we see in our calculations, we calculate the one-photon absorption spectrum of $MAPbBr_3$. We use the information on transition energies [Figs. 3(a) and 3(c)] and transition matrix elements throughout momentum space to calculate the absorption profile from first principles [Figs. 3(b) and 3(d)]. These represent the averaged value for all crystal directions to account for the polycrystallinity of our thin film in the experiments. At the band minima we observe one-photon transition strengths of approximately 6×10^3 cm^{-1} [Fig. 3(d)] at the surface, and approximately 8×10^2 cm^{-1} within the bulk [Fig. 3(b)]. This demonstrates that, even near the minima of the Rashba-split bands, optical transitions are still strongly allowed. However, for the bulk, the absorption coefficient shows a two-step behavior with a quick rise to approximately 8×10^2 cm^{-1} at the band edge and then an additional increase of more than one order of magnitude from band edge to the energy at the point of symmetry, $E_g(\mathbf{k} = R)$ [Fig. 3(b)], while at the surface the absorption increases more sharply, and reaches its maximum already close to the band edge [Fig. 3(d)]. This is due to a decreased joint density of states near the absorption onset for the bulk, which has stronger Rashba splitting. Additionally, for operational carrier densities of 10^{15} cm^{-3}, our calculated carrier distributions show that states around $E_g(\mathbf{k} = R)$ are significantly populated at room temperature

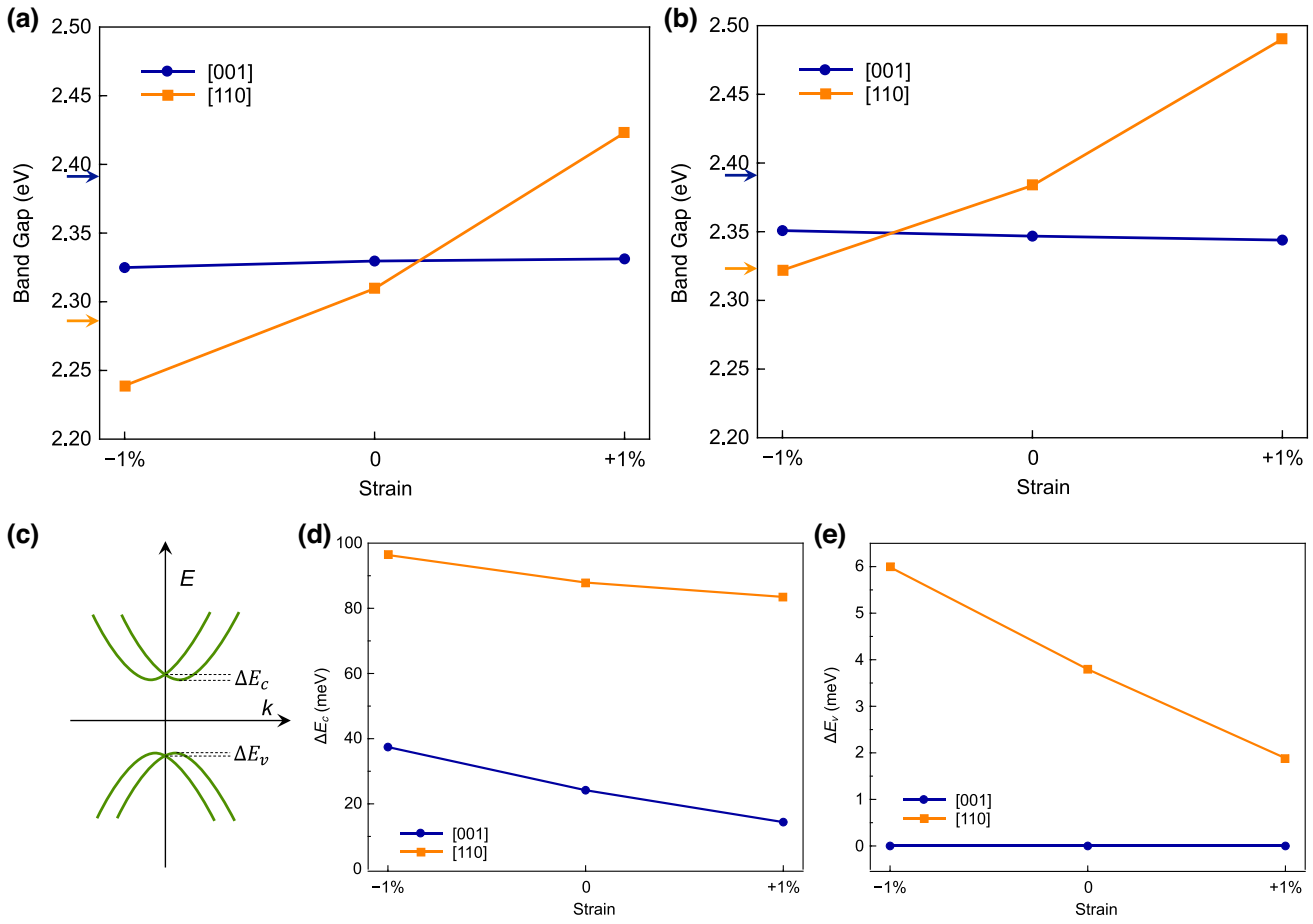

FIG. 4. (a),(b) Calculated lowest energy band gap (E_g) (a) and the band gap at $\mathbf{k} = R$ [$E_g(R)$] (b) of $MAPbBr_3$ with MA oriented along [001] and [110] as a function of the biaxial strain. The blue and orange arrows next to the y axis indicate the experimentally measured band gaps. Under −1% strain, the surface has greater band gaps than the bulk, which explains the experimentally observed larger band gap at the $MAPbBr_3$ surface than in the bulk. (c) Schematic band structure of $MAPbBr_3$, illustrating the Rashba splitting near the band extrema. ΔE_c and ΔE_v represent the Rashba splitting at the conduction-band minimum and valence-band maximum, respectively. (d),(e) Variations of ΔE_c and ΔE_v of $MAPbBr_3$ with MA oriented along [001] and [110] as a function of the biaxial strain. The Rashba splitting at the surface ([100] orientation) is always weaker than that in the bulk ([110] orientation), irrespective of strain.

(see Fig. S7 in the Supplemental Material [20]), such that the effects of band splitting on radiative recombination are reduced even further.

Unexpectedly, the experimentally observed larger band gap of the surface compared with the bulk is not reproduced using the crystal structures we assumed for our first-principles electronic structure calculations. Yet, these were performed for strain-free material. It has been experimentally demonstrated that a residual strain is present in the mixed halide perovskite thin films [34]. It is thus highly likely that our $MAPbBr_3$ thin films contain residual strain, which in turn impacts the band gaps. Hence, we explicitly compute the electronic structures of the $MAPbBr_3$ surface and bulk under biaxial strains of -1% (compressive), 0%, and 1% (tensile) [which are reasonable strain values as observed in experiments [34]], and the corresponding band gaps are summarized in Figs. 4(a) and 4(b). The band gap of $MAPbBr_3$ with the organic molecule MA oriented along [110] (the bulk scenario) decreases with compressive strain, while the band gap of $MAPbBr_3$ with MA along [001] (the surface scenario) is almost independent of strain. Under -1% compressive strain, both E_g and $E_g(R)$ of the $MAPbBr_3$ surface are greater than those of the bulk, consistent with experiment. We note that the relative strength of the Rashba splitting of $MAPbBr_3$ bulk and surface remains the same after taking the biaxial strains into account [Figs. 4(c)–4(e)].

III. CONCLUSIONS

Our findings report three key insights on the electronic states and charge-carrier dynamics in thin-film hybrid perovskites: (i) the band-gap energy in the bulk is lower compared to the surface; (ii) the Rashba-type band splitting is larger in the bulk compared to the surface; and (iii) fast radiative recombination occurs in the bulk from carrier funneling and strong one-photon transitions even from the extrema of Rashba-split bands.

We interpret the difference in optical band-gap energies as the existence of heterogeneity between the surface and the bulk electronic states, which we expect to drive charge-carrier transport away from the surface and thus reduce the impact of nonradiative carrier losses from surface defects [35]. Such heterogeneity would give rise to further charge extraction barriers, which highlights the importance of interfacial energy alignment of electron and/or hole extraction layers [2,3,36], and rationalizes charge-carrier buildup at device interfaces, despite rigorous optimization of electron transport layers [37], which leads to open-circuit voltage losses. Our results highlight the need to obtain the exact band alignment and band bending from built-in electric fields at the surface, e.g., from photoelectron microscopy for the surface, and, e.g., from optical absorption for the bulk. Our results further agree with depth-dependent band-gap profiling experiments, which found a strain gradient in MAPbI3 thin films from the surface to the bulk [27].

Our study unifies seemingly contradictory reports on varying levels of Rashba splitting and bright emission from the hybrid perovskites [12,38–41]. Our findings of an intrinsic heterogeneity between electronic states of the surface and bulk of the hybrid perovskite suggest that the material cannot be considered isotropic in its electronic structure, and that different results are to be expected from probing surface and bulk regions as reported [42,43]. Our first-principles calculations explain the bright luminescence from the bulk, despite the presence of Rashba-split bands, through the high quasi-Fermi energies of electrons and holes with respect to the high-symmetry point (R) at application-relevant carrier densities, as well as the relaxed optical selection rules from bands that we find to be no longer "pure" in their total angular momentum. Our results on energy gradients between surface and bulk have implications on the design of hybrid perovskite photovoltaics, which require alignment of charge extracting and/or injecting layers with the hybrid perovskites, as well as light-emitting applications, in which knowledge on recombination regions and charge-carrier densities is key for optimal design.

ACKNOWLEDGMENTS

S.A.B. and A.M. acknowledge the support from the EPSRC Centre for Doctoral Training in Graphene Technology (Grant No. EP/L016087/1). T.W., L.E., and F.D. acknowledge funding from an EPSRC NI grant (Grant No. EP/R044481/1). F.D. acknowledges support from the DFG Emmy Noether Programme (Project No. 387651688) and the Winton Programme for the Physics of Sustainability. T.W. received funding from the European Union's Horizon 2020 research and innovation program under Marie Skłodowska-Curie Grant Agreement No. 838772 (LADIE). S.F. acknowledges funding from the EPSRC and the Studienstiftung des deutschen Volkes. H.A. acknowledges studentship funding from the EPSRC and the Winton Programme for the Physics of Sustainability. X.Z. was supported by the National Natural Science Foundation of China (Grant No. 52172136). B.Z. and C.G.V.d.W. were supported by the U.S. Department of Energy (DOE), Office of Science, Basic Energy Sciences (BES) under Award No. DE-SC0010689. Computational resources were provided by the National Energy Research Scientific Computing Center, a DOE Office of Science User Facility supported by the Office of Science of the U.S. Department of Energy under Contract No. DE-AC02-05CH11231.

[1] S. D. Stranks and H. J. Snaith, Metal-halide perovskites for photovoltaic and light-emitting devices, Nat. Nanotechnol. **10**, 391 (2015).

[2] J. Jiménez-López, W. Cambarau, L. Cabau, and E. Palomares, Charge injection, carriers recombination and HOMO energy level relationship in perovskite solar cells, Sci. Rep. **7**, 1 (2017).
[3] S. Ravishankar, S. Gharibzadeh, C. Roldán-Carmona, G. Grancini, Y. Lee, M. Ralaiarisoa, A. M. Asiri, N. Koch, J. Bisquert, and M. K. Nazeeruddin, Influence of charge transport layers on open-circuit voltage and hysteresis in perovskite solar cells, Joule **2**, 788 (2018).
[4] M. Stolterfoht, Pietro Caprioglio, Christian M. Wolff, José A. Márquez, Joleik Nordmann, Shanshan Zhang, Daniel Rothhardt, Ulrich Hörmann, Yohai Amir, Alex Redinger, Lukas Kegelmann, Fengshuo Zu, de Steve Albrecht, Norbert Koch, de Thomas Kirchartz, Michael Saliba, Thomas Unold, and Dieter Neher, The impact of energy alignment and interfacial recombination on the internal and external open-circuit voltage of perovskite solar cells, Energy Environ. Sci. **12**, 2778 (2019).
[5] C. M. Wolff, P. Caprioglio, M. Stolterfoht, and D. Neher, Nonradiative recombination in perovskite solar cells: The role of interfaces, Adv. Mater. **31**, 1902762 (2019).
[6] I. Zarazua, J. Bisquert, and G. Garcia-Belmonte, Light-induced space-charge accumulation zone as photovoltaic mechanism in perovskite solar cells, J. Phys. Chem. Lett. **7**, 525 (2016).
[7] F. Zheng, L. Z. Tan, S. Liu, and A. M. Rappe, Rashba spin-orbit coupling enhanced carrier lifetime in $CH_3NH_3PbI_3$, Nano Lett. **15**, 59 (2015).
[8] J. M. Richter, M. Abdi-Jalebi, A. Sadhanala, M. Tabachnyk, J. P. H. Rivett, L. M. Pazos-Outón, K. C. Gödel, M. Price, F. Deschler, and R. H. Friend, Enhancing photoluminescence yields in lead halide perovskites by photon recycling and light out-coupling, Nat. Commun. **7**, 13941 (2016).
[9] F. Deschler, Michael Price, Sandeep Pathak, Lina E. Klintberg, David-Dominik Jarausch, Ruben Higler, Sven Hüttner, Tomas Leijtens, Samuel D. Stranks, Henry J. Snaith, Mete Atatüre, Richard T. Phillips, and Richard H. Friend, High photoluminescence efficiency and optically pumped lasing in solution-processed mixed halide perovskite semiconductors, J. Phys. Chem. Lett. **5**, 1421 (2014).
[10] C. L. Davies, M. R. Filip, J. B. Patel, T. W. Crothers, C. Verdi, A. D. Wright, R. L. Milot, F. Giustino, M. B. Johnston, and L. M. Herz, Bimolecular recombination in methylammonium lead triiodide perovskite is an inverse absorption process, Nat. Commun. **9**, 293 (2018).
[11] C. Wehrenfennig, G. E. Eperon, M. B. Johnston, H. J. Snaith, and L. M. Herz, High charge carrier mobilities and lifetimes in organolead trihalide perovskites, Adv. Mater. **26**, 1584 (2014).
[12] X. Zhang, J. X. Shen, W. Wang, and C. G. Van de Walle, First-principles analysis of radiative recombination in lead-halide perovskites, ACS Energy Lett. **3**, 2329 (2018).
[13] X. Zhang, J. X. Shen, and C. G. Van de Walle, Three-dimensional spin texture in hybrid perovskites and its impact on optical transitions, J. Phys. Chem. Lett. **9**, 2903 (2018).
[14] C. Stavrakas, A. A. Zhumekenov, R. Brenes, M. Abdi-Jalebi, V. Bulović, O. M. Bakr, E. S. Barnard, and S. D. Stranks, Probing buried recombination pathways in perovskite structures using 3D photoluminescence tomography, Energy Environ. Sci. **11**, 2846 (2018).
[15] B. Wu, H. T. Nguyen, Z. Ku, G. Han, D. Giovanni, N. Mathews, H. J. Fan, and T. C. Sum, Discerning the surface and bulk recombination kinetics of organic-inorganic halide perovskite single crystals, Adv. Energy Mater. **6**, 1600551 (2016).
[16] K. Jung Karki, M. Abdellah, W. Zhang, and T. Pullerits, Different emissive states in the bulk and at the surface of methylammonium lead bromide perovskite revealed by two-photon micro-spectroscopy and lifetime measurements, APL Photonics **1**, 46103 (2016).
[17] J. J. Hopfield, J. M. Worlock, and K. Park, Two-quantum absorption spectrum of KI, Phys. Rev. Lett. **11**, 414 (1963).
[18] J. J. Hopfield and J. M. Worlock, Two-quantum absorption spectrum of KI and CsI, Phys. Rev. **137**, A1455 (1965).
[19] S. Polishchuk, Michele Puppin, Alberto Crepaldi, Gianmarco Gatti, Dmitry N. Dirin, Olga Nazarenko, Nicola Colonna, Nicola Marzari, Maksym V Kovalenko, Marco Grioni, and Majed Chergui, Nanoscale-resolved surface-to-bulk electron transport in $CsPbBr_3$ perovskite, Nano Lett. **2022**, 1067 (2022).
[20] See Supplemental Material at http://link.aps.org/supplemental/10.1103/PRXEnergy.3.033001 for experimental and theoretical methodological details, and additional spectroscopic data and calculated carrier occupation, which contains additional references [21–26].
[21] G. Kresse and J. Furthmüller, Efficient iterative schemes for *ab initio* total-energy calculations using a plane-wave basis set, Phys. Rev. B **54**, 11169 (1996).
[22] P. E. Blochl, Projector augmented-wave method, Phys. Rev. B **50**, 24 (1994).
[23] J. Heyd, G. E. Scuseria, and M. Ernzerhof, Hybrid functionals based on a screened Coulomb potential, J. Chem. Phys. **118**, 8207 (2003).
[24] H. J. Monkhorst and J. D. Pack, Special points for Brillouin-zone integrations, Phys. Rev. B **13**, 5188 (1976).
[25] F. Chen, C. Zhu, C. Xu, P. Fan, F. Qin, A. Gowri Manohari, J. Lu, Z. Shi, Q. Xu, and A. Pan, Crystal structure and electron transition underlying photoluminescence of methylammonium lead bromide perovskites, J. Mater. Chem. C **5**, 7739 (2017).
[26] S. Brittman and E. C. Garnett, Measuring n and k at the microscale in single crystals of CH_3NH_3 $PbBr_3$ perovskite, J. Phys. Chem. C **120** (1), 616 (2016).
[27] Y. Yang, M. Yang, D. T. Moore, Y. Yan, E. M. Miller, K. Zhu, and M. C. Beard, Top and bottom surfaces limit carrier lifetime in lead iodide perovskite films, Nat. Energy **2**, 1 (2017).
[28] S. Kanno, Y. Imamura, A. Saeki, and M. Hada, Rotational energy barriers and relaxation times of the organic cation in cubic methylammonium lead/tin halide perovskites from first principles, J. Phys. Chem. C **121**, 14051 (2017).
[29] A. Johnston, G. Walters, M. I. Saidaminov, Z. Huang, K. Bertens, N. Jalarvo, and E. H. Sargent, Bromine incorporation and suppressed cation rotation in mixed-halide perovskites, ACS Nano **17**, 48 (2020).
[30] C. A. López, M. V. Martínez-Huerta, M. C. Alvarez-Galván, P. Kayser, P. Gant, A. Castellanos-Gomez, M. T. Fernández-Díaz, F. Fauth, and J. A. Alonso, Elucidating

the methylammonium (MA) conformation in $MAPbBr_3$ perovskite with application in solar cells, Inorg. Chem. **56**, 14214 (2017).

[31] C. A. López, M. C. Álvarez-Galván, M. V. Martínez-Huerta, M. T. Fernández-Díaz, and J. A. Alonso, Dynamic disorder restriction of methylammonium (MA) groups in chloride-doped $MAPbBr_3$ hybrid perovskites: A neutron powder diffraction study, Chem. Eur. J. **25**, 4496 (2019).

[32] F. Zu, P. Amsalem, M. Ralaiarisoa, T. Schultz, R. Schlesinger, and N. Koch, Surface state density determines the energy level alignment at hybrid perovskite/electron acceptors interfaces, ACS Appl. Mater. Interfaces **9**, 41546 (2017).

[33] Y. Rakita, O. Bar-Elli, E. Meirzadeh, H. Kaslasi, Y. Peleg, G. Hodes, I. Lubomirsky, D. Oron, D. Ehre, and D. Cahen, Tetragonal $CH_3NH_3PbI_3$ is ferroelectric, Proc. Natl. Acad. Sci. U. S. A. **114**, E5504 (2017).

[34] C. Zhu, *et al.*, Strain engineering in perovskite solar cells and its impacts on carrier dynamics, Nat. Commun. **10**, 1 (2019).

[35] H. Jin, E. Debroye, M. Keshavarz, I. G. Scheblykin, M. B. J. Roeffaers, J. Hofkens, and J. A. Steele, It's a trap! On the nature of localised states and charge trapping in lead halide perovskites, Mater. Horiz. **7**, 397 (2020).

[36] R. A. Belisle, P. Jain, R. Prasanna, T. Leijtens, and M. D. McGehee, Minimal effect of the hole-transport material ionization potential on the open-circuit voltage of perovskite solar cells, ACS Energy Lett. **1**, 556 (2016).

[37] S. Pisoni, M. Stolterfoht, J. Löckinger, T. Moser, Y. Jiang, P. Caprioglio, D. Neher, S. Buecheler, and A. N. Tiwari, On the origin of open-circuit voltage losses in flexible n-i-p perovskite solar cells, Sci. Technol. Adv. Mater. **20**, 786 (2019).

[38] T. Etienne, E. Mosconi, and F. De Angelis, Dynamical origin of the Rashba effect in organohalide lead perovskites: A key to suppressed carrier recombination in perovskite solar cells?, J. Phys. Chem. Lett. **7**, 1638 (2016).

[39] T. Wang, B. Daiber, J. M. Frost, S. A. Mann, E. C. Garnett, A. Walsh, and B. Ehrler, Indirect to direct bandgap transition in methylammonium lead halide perovskite, Energy Environ. Sci. **10**, 509 (2017).

[40] S. D. Stranks and P. Plochocka, The influence of the Rashba effect, Nat. Mater. **17**, 381 (2018).

[41] E. M. Hutter, M. C. Gélvez-Rueda, A. Osherov, V. Bulović, F. C. Grozema, S. D. Stranks, and T. J. Savenije, Direct-indirect character of the bandgap in methylammonium lead iodide perovskite, Nat. Mater. **16**, 115 (2017).

[42] O. Schuster, Peter Wientjes, Shreetu Shrestha, Ievgen Levchuk, Mykhailo Sytnyk, Gebhard J. Matt, Andres Osvet, Miroslaw Batentschuk, Wolfgang Heiss, Christoph J. Brabec, Thomas Fauster, and Daniel Niesner, Looking beyond the surface: The band gap of bulk methylammonium lead iodide, Nano Lett. **20**, 3090 (2020).

[43] H. P. Pasanen, P. Vivo, L. Canil, H. Hempel, T. Unold, A. Abate, and N. V. Tkachenko, Monitoring charge carrier diffusion across a perovskite film with transient absorption spectroscopy, J. Phys. Chem. Lett. **11**, 445 (2020).